MONTE CARLO ELECTROMAGNETIC CROSS SECTION PRODUCTION METHOD FOR LOW ENERGY CHARGED PARTICLE TRANSPORT THROUGH SINGLE MOLECULES

A Thesis

by

JONATHAN ROBERT MADSEN

Submitted to the Office of Graduate Studies of
Texas A&M University
in partial fulfillment of the requirements for the degree of

MASTER OF SCIENCE

Chair of Committee,	Gamal Akabani
Co-Chair of Committee,	John Ford
Committee Members,	Lisa Perez
Head of Department,	Yassin Hassan

August 2013

Major Subject: Nuclear Engineering

ABSTRACT

The present state of modeling radio-induced effects at the cellular level neglects to account for the microscopic inhomogeneity of the nucleus from the non-aqueous contents by approximating the entire cellular nucleus as a homogenous medium of water. Charged particle track-structure calculations utilizing this principle of superposition are thereby neglecting to account for approximately 30% of the molecular variation within the nucleus. To truly understand what happens when biological matter is irradiated, charged particle track-structure calculations need detailed knowledge of the secondary electron cascade, resulting from interactions with not only the primary biological component – water – but also the non-aqueous contents, down to very low energies.

This paper presents developments for a novel approach, which to our knowledge has never been done before, to reducing the homogenous water approximation. The purpose of our work is to develop of a completely self-consistent computational method for predicting molecule-specific ionization, excitation, and scattering cross sections in the very low energy regime that can be applied in a condensed history Monte Carlo track-structure code. The present methodology begins with the calculation of a solution to the many-body Schrödinger equation and proceeds to use Monte Carlo methods to calculate the perturbations in the internal electron field to determine the aforementioned processes. Results are computed for molecular water in the form of linear energy loss, secondary electron energies, and ionization-to-excitation ratios and compared against the low energy predictions of the GEANT4-DNA physics package of the Geant4 simulation toolkit.

DEDICATION

I dedicate this thesis to my father and mother, who always put their children first and never compromised in ensuring we were in the best situation to receive the best education possible.

Ad Majorem Dei Gloriam

ACKNOWLEDGEMENTS

I would like to extend my gratitude to my graduate advisor and committee chair, Dr. Gamal Akabani, without his faith in my abilities I would not be here today. I would also like to thank my committee members: Dr. John Ford and Dr. Lisa Perez for all their assistance.

I would also like to thank Dr. Sébastian Incerti of the Geant4-DNA collaboration, who proposed my membership to the Geant4 collaboration as a member of the Geant4-DNA project that provided me with much of the inspiration for this vein of scientific inquiry. Additionally, I would like to thank some of my fellow graduate students, Michael Hackemack and Arnulfo Gonzalez, who have been instrumental through their contributions of ideas and insights.

TABLE OF CONTENTS

Page

LIST OF FIGURES

Page

LIST OF TABLES

Page

1. INTRODUCTION

1.1 Paradigm

The electromagnetic force governs the low-energy physics domain, as collisional interactions between nuclei are statistically improbable. Prior work has demonstrated the validity of using the solution to the many-body Schrödinger equation in solving the absolute electron-impact ionization cross section of molecules (Deutsch, Becker, Matt, & Mark, 1999; Huang, Kim, & Rudd, 1996; Irikura & Karl, 2000). However, the methods currently employed for absolute electron-impact ionization cross-sections provide no "details of the resonances in the continuum, or vibrational and/or rotational excitations concomitant with ionization, multiple ionization, dissociative ionization, etc. It simply predict the total ionization cross section as the sum of ionization cross sections for ejecting one electron from each of the atomic or molecular orbital" (Huang, Kim, & Rudd, 1996). In other words, the methods are limited to the calculation of the total ionization cross section only. Other models, such as those developed by Champion (2003), extend their predictions to multiple ionizations, dissociative ionization, vibrational excitation, etc. but are limited to the liquid-vapor water molecule as described in Champion (2003). As computational power increases and particle theory progresses, highly accurate simulations of the effect of ionizing radiation are within our computational grasp.

The widely employed Monte Carlo method for nuclear physics simulations provides and excellent computational environment for simulations accounting for the highly

probabilistic nature of particle physics interactions. However, the verification barrier lies in determining the associated probabilities of interaction that are inherently difficult, if at all possible, to measure experimentally at low energies (Pimblott & LaVerne, 2007).

The current paradigm associated with Monte Carlo "track structure" simulations of charged particle ionizing radiation in the cellular environment employs an approximation called the "principle of superposition". Within this approximation, the cellular nucleus is treated as a homogeneous medium of water. The track structure calculations of the incident charged particle and secondary electrons liberated from ionization processes within the medium are done via Monte Carlo transport without the presence of the DNA or proteins residing within the nucleus. Advanced simulation codes, such as Geant4-DNA and PARTRAC (Friedland, Dingfelder, Kundrat, & Jaboc, 2011), also compute the production and diffusion of water radicals arising from the incident charged particle. Once the track structure has been produced, the non-aqueous contents of the cellular nucleus are overlaid onto the track structure. Secondary electrons and water radicals produced in the region occupied by the DNA and proteins are discarded and direct DNA strand breaks are approximated as having occurred in that localized region of the DNA strand. The objective of this work is to develop a computational framework for computing the low energy cross sections of single molecules such that the molecules composing the non-aqueous contents of the cellular nuclei can be included directly in the simulation and thereby remove the approximation of the principle of superposition.

As will be revealed in this paper, the methodology employed involves the inclusion of a solution to the many-body Schrödinger equation for the electron probability density and vibrational character of single molecules and employing a perturbation-type theory on the molecule to determine the ionization and excitation characters of the molecule when subject to charged particle irradiation. While the future goal is fully encompass all possible physical processes, this work is preliminary to the full scope and is thus limited to these predictions.

1.2 Previous Approaches

Inquiries into the method of interaction between incident charged particles and atoms and molecules using quantum mechanical theory dates back to the 1930's under Bethe and his successful development of a theory of the stopping power of materials for fast particles (Chan, 2007). Bethe's description regards the collision as the sudden transfer of momentum and energy to atomic electrons (Chan, 2007). To summarize the more detailed description found in Champion (2003, Phys. Med. Biol. 48), as experimental ionization data became more readily available, subsequent evolution of Bethe's original theory later developed into the "binary-encounter-dipole" (BED) by Kim *et al* (Kim and Rudd 1994, 1999, Hwang et al. 1996), which combined Bethe's theory with the binary-encounter theory developed by Vriens (1969). This model required knowledge of the optical oscillator strength and due to the lack of experimental data Kim *et al* subsequently proposed the binary-encounter-Bethe (BEB) model as an improvement on the BED model. However, the deficiencies of both models are their reliance on semi-empirical descriptions of the ionization process and they were limited to singly

differential and total ionization cross section calculations. An extension by Coimbra and Barbieri (1997) extended the BEB model to calculate the doubly differential cross sections (with respect to incident particle energy and molecular orbital subshells) by reducing the number of adjustable parameters in Rudd's model from eight to three – electron binding energy, the average kinetic energy, and the electron occupation number of the subshell (Seo, Pia, Saracco, & Kim, 2010). Low-energy cross section production progress at this point has dependencies on semi-empirical data, twice differentiable, and uncertainty at low incident particle kinetic energies relative to the kinetic energy of the atomic or molecular electrons. Most recently, the extensive work by Champion, et al. (2001, 2002, 2003) has developed a new approach resulting an eight-fold differential cross section over the orientation of the target molecule (Euler angles α, β, and γ), scattered direction ($\Omega_s = \sin\theta_s\, d\theta_s\, d\varphi_s$), ejected direction ($\Omega_e = \sin\theta_e\, d\theta_e\, d\varphi_e$), and energy transfer ($dE_e$) (Champion, 2003). The framework of Champion (2003) describes incident and scattered (fast) electrons by a plane wavefunction and ejected (slow) electrons by a distorted wavefunction. The distorted wavefunction of an ejected electron is a solution of the radial Schrödinger equation in which the effective distortion potential is calculated for each molecular orbital. The description of the water molecule used by Champion (2003) provides the description of the molecular orbitals for water summarized in Table 1, which also lists the description of the molecular orbitals utilized in our calculations. The Champion (2003) methodology has been implemented in Geant4-DNA and is used for benchmarking with our methodology.

Table 1 Ionization Potentials of the 5 Occupied Molecular Orbitals of H_2O

IP_{vapor} [a]	IP_{liquid} [a]	IP_{liquid} [b]
12.6 eV	8.8 eV	8.884 eV
14.7 eV	12.1 eV	10.989 eV
18.4 eV	16.8 eV	14.606 eV
32.2 eV	32.2 eV	27.807 eV
532.0 eV	532.0 eV	521.426 eV

[a] Champion (2003)

[b] B3LYP (aug-cc-pVDZ) with PCM correction to liquid state (see *Computational Chemistry* Section)

2. METHODOLOGY

The following methodology has been implemented in C++. The Monte Carlo method consists of a simulation defined as a single molecule being subjected to incident charged particles of a distribution of initial kinetic energies. The simulation program is preliminarily being called Monte Carlo Molecular Transport (MCMT). The methodology is the first iteration in our attempt to determine a generic model for producing low-energy electromagnetic cross sections that after calculation can be implemented in a condensed history Monte Carlo code such as Geant4 or MCNP. The methodology is a radical shift from the current treatments of theoretically determining low-energy electromagnetic cross sections because it accounts for the shape and probability distributions of the electrons in molecular orbitals via the solution to the many-body Schrödinger equation. This thesis is theoretical and should be interpreted as an initial approach that may lead to an entirely new method of low-energy cross section prediction as the methodology becomes more refined in future work. With this assertion, it should be understood that this methodology has its limitations; however, it does contain some valuable insights into our development. The simulation is designed for any incident charged particle (e.g. H^+, He^+, He^{++}) but time constraints have limited our analysis to only incident electrons. The following section gives an overview of the simulation algorithm and the setting of the simulation (default setting contained in […]):

2.1 Simulation

2.1.1 Simulation Overview

I. Initialize Base Geometry

a. Build world container volume

II. Initialize Physical Molecule

a. Read custom file describing molecule

i. Orbital Energies

ii. Vibrations

iii. Number of electrons

iv. GAUSSIAN cube files

1. Position mapping matrix for electron probabilities

2. Generate mesh of electron probability discretization

3. Create nuclei

4. Create Molecular Orbitals and Spin Pairs

a. Create classes for handling 3D acceptance-rejection technique of probabilities (see *Three-Dimensional Rejection Technique* section)

b. Create physical electrons and place in orbitals

c. Assign quantum numbers to orbital electrons

b. Compute gradient fields for molecule

c. Organize mesh volume hierarchy

i. Mesh wrapper class – contains all mesh sections

ii. Mesh section class – contains a partition of mesh volumes

iii. Mesh volume class – smallest element of mesh

2.1.2 Simulation Settings

- Maximum number of steps [100,000] (see *Stepping Algorithm* section)
- Energy distribution of starting energies [Base-10 Logarithmic bins, Linear distribution across bins]
- Integration Method [4^{th} order Runge-Kutta]
- Maximum number of ionization/dissociative ionization events before killing particle [3]
- World dimensions [For water molecule: 0.62 x 0.62 x 0.62 nm]
    - Based on ~3.2 angstroms between water molecules at standard density
- Minimum Cutoff Energy before killing particle [4 eV for electrons]
- Vibration Modes [All vibration modes with equal weight]
- Maximum simulation energy [1 keV]
- Real time force [ON]
    - Averages precompiled gradient force field with instantaneous force of molecular nuclei at vibrational position and molecular electrons at their sampled position
- Scale excitation energies [ON]
    - Excitation energies are scaled by the sum of all excitation energies for the step to the incident particle energy (incident particle cannot give up more kinetic energy than it has)

2.2 Computational Chemistry

The computational chemistry code GAUSSIAN 09 was used to determine the electron probability density, molecular vibrational frequencies, molecular orbital binding energies, and molecular orbital kinetic energies (Frisch, et al., 2009). The level of theory used was the density functional theory (DFT) method called B3LYP (Becke, 1988; Lee, Yang, & Parr, 1988). The basis set used for these computations was correlation-consistent polarized valence double zeta with diffuse functions (aug-CCPVDZ) (Woon & Dunning, Jr., 1995). Corrections for long-range electrostatic forces imposed by the solvation of the molecule were accounted for by using the polarizable continuum model (PCM) (Tomasi, Mennuci, & Cammi, 2005).

2.2.1 Orbital Energies and Vibrational Frequencies

Vibrational frequency modes of the atomic nuclei and the molecular orbital binding and kinetic energies were extracted from the GAUSSIAN (B3LYP/aug-cc-pVDZ) results. The molecular orbitals have two energies values – binding energy of the orbital, which are critical in estimating the ionization potential of the electrons occupying the orbital (see *Ionization* section), and kinetic energy, which are critical in determining the step length of the incident particle with respect to molecular orbital (see *Stepping Algorithm* section). One vibrational mode has four critical values: harmonic frequency (cm^{-1}), force constant (mDyne/Å), reduced mass (AMU), and normal coordinate. The harmonic frequency (k), also known as the wave number, is analogous to energy via:

$$E = \hbar c k \tag{1}$$

where $\hbar$ is the reduced Planck's constant and c is the speed of light. The frequency of vibration is defined as:

$$f = \sqrt{\frac{F_c}{m_R}} \tag{2}$$

where m_R is the reduced mass, and F_c is the force constant. The amplitude A of the vibration is:

$$A = \sqrt{\frac{\hbar}{m_R \omega}} \tag{3}$$

where ω is the angular frequency equivalent to $2\pi f$. These values in combination with the normal coordinate vector ($\vec{n}, \vec{A} = A\vec{n}$) produce oscillations about the equilibrium point ($\vec{X}_0$ – see G*AUSSIAN Cube Files* section) according to:

$$\vec{x}(t) = \vec{A}\cos(\omega t) - \vec{X}_0 \tag{4}$$

The time value t is set with the incident particle lifetime, which is logarithmically randomized over 1×10^{-12} seconds, at the time of creation to ensure the molecule is in various vibrational phases at the time of creation. Additionally, the specific mode of vibration is randomly selected at the creation of the particle and held in that specific mode during the time lapse of the incident particle transport. The vibrational modes and normal coordinates for the H_20 molecule can be found in Table 2 and 3, respectively.

Table 2 Frequency, Reduced Masses, and Force Constants for 3 Vibrational Modes of Water

	Mode 1	Mode 2	Mode 3
Frequency (cm^{-1})	1609.6017	3781.9628	3878.0327
Reduced Mass (AMU)	1.082	1.0458	1.0816
Force Constant (mDyne/Å)	97.6870	16.9809	103.889

Table 3 Normal Coordinates for 3 Vibrational Modes of Water

		Mode 1			Mode 2			Mode 3		
Atom	AN	X	Y	Z	X	Y	Z	X	Y	Z
1	8	0.00	0.00	0.07	0.00	0.00	0.05	0.00	0.07	0.00
2	1	0.00	-0.43	-0.56	0.00	0.58	-0.40	0.00	-0.56	0.43
3	1	0.00	0.43	-0.56	0.00	-0.58	-0.40	0.00	-0.56	-0.43

2.2.2 GAUSSIAN Cube Files

Using the GAUSSIAN "cubegen" utility, a mesh was generated for each occupied orbital of the molecule. These meshes provide the physical boundaries of the molecule and the localized electron density probabilities. The electron density probabilities for each orbital were normalized to unity with their occupation number, e.g. a $1s^2$ orbital is normalized to a value of 2.

GAUSSIAN cube files per orbital describe 7 components:

1. Number of atoms in molecule and origin of position transformation matrix
2. Number of voxels in X direction (N_x) and X axis vector
3. Number of voxels in Y direction (N_y) and Y axis vector
4. Number of voxels in Z direction (N_z) and Z axis vector
5. Molecular nuclei and their coordinates
6. Fragment number and orbital number
7. Electron probability density solutions of XYZ mesh

The position transformation matrix is composed of the X-, Y-, and Z-axis vectors in the form:

$$T = \begin{pmatrix} X_x & X_y & X_z \\ Y_x & Y_y & Y_z \\ Z_x & Z_y & Z_z \end{pmatrix} \tag{5}$$

The coordinates of the sampled electron is then:

$$V = T\begin{pmatrix} \xi_x \\ \xi_y \\ \xi_z \end{pmatrix} + \begin{pmatrix} O_x \\ O_y \\ O_z \end{pmatrix} \tag{6}$$

where the matrix O represents the coordinates of the origin, $\bar{\xi}$ represents the randomly selected X, Y, and Z voxel decided on by electron probability density solution (see *Three-Dimensional Rejection Technique* section). The exact position of the electron within the voxel is randomly distributed within the boundaries of the voxel so the

instantaneous force of the electron on a transported particle is not biased to an electron position at the exact center of the voxel.

2.2.2.1 Molecular Nuclei, Fragment Number, and Orbital Number

The molecular nuclei are described by their atomic number, charge, and X, Y, Z equilibrium positions. The coordinates of the equilibrium positions are stored for use when solving the position of the nuclei in their vibrational modes. The fragment number is discarded as this value pertains to an ID assigned by GAUSSIAN when constructing a larger chain of molecules. The orbital number represents an ID number assigned by GAUSSIAN for each electron pair composing an orbital. These ID values are assigned by their binding energy where an ID of 1 represents the most tightly bound electron pair.

2.2.2.2 Electron Probability Density Solution

The bulk of the information in the GAUSSIAN cube file is the electron probability density solution consisting of $N_xN_yN_z$ entries (see Figure 1). The entries, according to the exclusion principle stating that two electrons cannot occupy the same point in space and the same quantum numbers, are denoted as positive or negative and the square of the entry represents the probability the electron exists at that point in space. By recording the sign of the entry, one can determine the orbital *+1/2* or *-1/2* spin type (arbitrarily decided as positive values are *+1/2* spin and vice versa) and the square of the probability is stored. The entire list of entries is normalized to 1 for each molecular orbital in the molecular orbital spin pair.

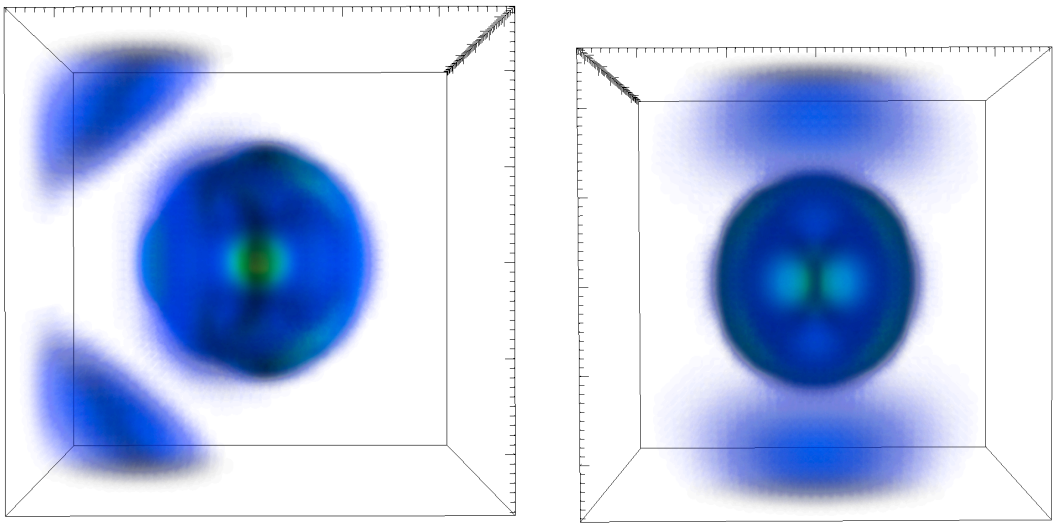

Figure 1 Electron Probability Density of All H_2O Molecular Orbitals. -- YZ plane with oxygen at center, hydrogen atoms at upper left and lower left positions (left), XY plane with oxygen at center, hydrogen atoms at top center and bottom center (right)

2.2.3 Three-Dimensional Rejection Technique

The most efficient method of determining probabilistic coordinates in a three dimensional space is composing two additional matrices in addition to the full three-dimensional probability matrix. The acceptance-rejection algorithm for a one-dimensional matrix utilizes two random numbers. The first random number is an integer value $\xi_1 \in [0, N)$ where N is the number of entries in the matrix. The second random number is a floating-point number between $\xi_2 \in [0, max)$ where the maximum is the largest value within the one-dimensional matrix (this assumes all entries are positive). If the matrix entry at ξ_1 is greater than ξ_2 the index ξ_1 is accepted, if ξ_2 is greater than the matrix entry at ξ_1, two new random numbers are generated and the process is repeated.

Given the three-dimensional matrix, the first of the two additional matrices is composed by collapsing the matrix into two dimensions, e.g. for each one-dimensional matrix at a given Z and Y index of the matrix, the matrix is summed into one value and that sum is the new value at the given Z and Y index of the matrix. This new two-dimensional matrix is then collapsed into a one-dimensional matrix in the same fashion. The result is three matrices – a one-dimensional matrix where the entries are the collapsed version of the other two dimensions (A), a two-dimensional matrix where the entries are the collapse of one of the dimensions (B) and the original three-dimensional matrix (C). The acceptance-rejection technique is then applied to A and an index (a) of the matrix is selected. The algorithm then proceeds to apply another acceptance-rejection technique to B at the row (a) and selects the next index (b). Finally, the algorithm processed to apply an acceptance-rejection technique to C at the indexes (a) and (b) and produces a third index (c). The result is three coordinate indexes (a)(b)(c) which are then applied to the position transformation matrix (described in the GAUSSIAN Cube Files section) to obtain the sampled position of the electron.

2.3 Molecular Force Field

Two meshes of Coulombic force fields were generated for our Monte Carlo transport method, one for the incident charged particle and another for the molecular electrons.

In order to account for the electromagnetic interaction between the incident charged particle and the electron cloud as a whole, rather than a completely instantaneous interaction of molecular electrons at randomly sampled positions, the force field for the incident particles is computed using the principle of superposition of the

Coulombic force via the summation of the Coulombic force from electrons at all possible positions within the mesh, weighted by the total probability that an electron "exists" at that location within the mesh. In other words, the force within the voxel is the superposition of a field of point charges where the magnitude accounts for the probability the point charge is there. The Coulombic forces from the molecular nuclei are computed for during runtime due to the variance in position due to molecular vibrations.

In order to compute the perturbation in the electromagnetic field of the molecule, the second force field for the molecular electrons is computed for each voxel within the mesh via the superposition of the Coulombic force between an electron within the current voxel, weighted by the total probability an electron exists within this voxel, and an electron within another voxel, also weighted by the total probability an electron exists within that voxel.

The matrix dimensions of the molecular electron field are identical to the probability density mesh generated by GAUSSIAN. The matrix dimensions of the second set are created by vertex computations on the first set, i.e. the molecular electron field discretized as a 31 x 31 x 31 mesh determines the incident particle field to be discretized as a 32 x 32 x 32 mesh. The force within each voxel *i* in the molecular electron mesh is defined as:

$$F_i = \sum_{j=0}^{N} P_i P_j k_e q_e q_0 \frac{R_{12}}{r_{12}^2} (i \neq j) \tag{7}$$

where P_i is the probability the electron exists in i, P_j is the probability an electron exists in j, k_e is the Coulomb constant, q_e is the fundamental charge of an electron, q_0 is the fundamental charge of a positron, R_{12} is the normalized direction from i to j, and r_{12} is the magnitude of the vector from i to j. N is the total number of voxels in mesh. The force within each voxel i of the incident particle mesh is defined as:

$$F_i = \sum_{j=0}^{N} P_j k_e q_e q_0 \frac{R_{12}}{r_{12}^2} \tag{8}$$

where N is the number of voxels in the molecular electron mesh, i.e. the force within the voxels of the incident particle mesh are independent of each other. Another key difference to note between the Eqn. (7) and (8) is the molecular electron field includes a second weight (Eqn. 7), which is the probability that the molecular electron exists within the voxel being computed.

This approach is an effort to accurately simulate the incident particle interaction in the scope of the electron probability density distribution instead of discrete electrons in a classical sense while avoiding the complex recalculation of the many-body Schrödinger equation. Future developments under investigation include the propagation of shifts in the electron density probabilities in accordance to perturbations in the electromagnetic field if the benefits exceed the computational requirements.

2.4 Stepping Algorithm

One of the most crucial developments of this model was the stepping algorithm for transport of the incident particle with respect to the movement of the molecular electrons. Since the magnitude of the velocity of the electrons within in the orbitals varies with respect to Coulombic potential of the nuclei, a constant value relating to the movement of the molecular electrons for each orbital is needed. The solution is the utilization of kinetic energy of the molecular orbital. In the final stages of geometrical construction, a time step parameter for the incident particle is defined as the time a particle traveling at the speed of light would require to traverse the diameter of the world volume:

$$t_s = \frac{2R_w}{c} \tag{9}$$

where R_w is the radius of the world volume and c is the speed of light. A table of step lengths for each orbital is computed via a comparison of the kinetic energy of the incident particle and the kinetic energy of the orbital:

$$\Delta x_0 = v_p t_s \sqrt{\frac{KE_p m_e}{KE_o m_p}} \tag{10}$$

where Δx_0 is the step length of the incident particle with respect to the molecular orbital, v_p is the velocity of the incident particle, t_s is the time step, m_e is the mass of an electron, m_p is the mass of the incident particle KE_p is the kinetic energy of the particle, and KE_O is the kinetic energy of the orbital. This table is fed to a C++ class designed to

keep track of two sets of data: the first set is the master set of step lengths with respect to each orbital, the second set is a scaled table of step lengths whose respective values never exceed the master table of step lengths and are scaled down each time a minimum step is requested from the stepping algorithm. In this fashion, the incident particle is stepped the appropriate number of times and distances with respect to each orbital. To ensure continuity across changes in kinetic energy of the incident particle, the relative data set is rescaled each time a new master data set is provided:

$$S_{i,n+1} = S_{i,n} \frac{R_{i,n+1}}{R_{i,n}} \tag{11}$$

where S represents the adjusted step lengths, R represents the master step lengths, i signifies the orbital number and n signifies the iteration number. Figure 2 provides a visual representation.

However, this description of stepping and evaluation of the molecular orbital selected via the smallest scaled step length is marginally incomplete. Following the selection of step distance and molecular orbital(s), the incident particle should be returned to it's original location since the incident particle was last stepped with respect to that selected orbital and the perturbed force field should reflect the state at that point in time. This would require a history of perturbed force field states for each orbital and this approach is not practical due to the increase in memory consumption arising in molecules such as adenine and solution has not been developed to date.

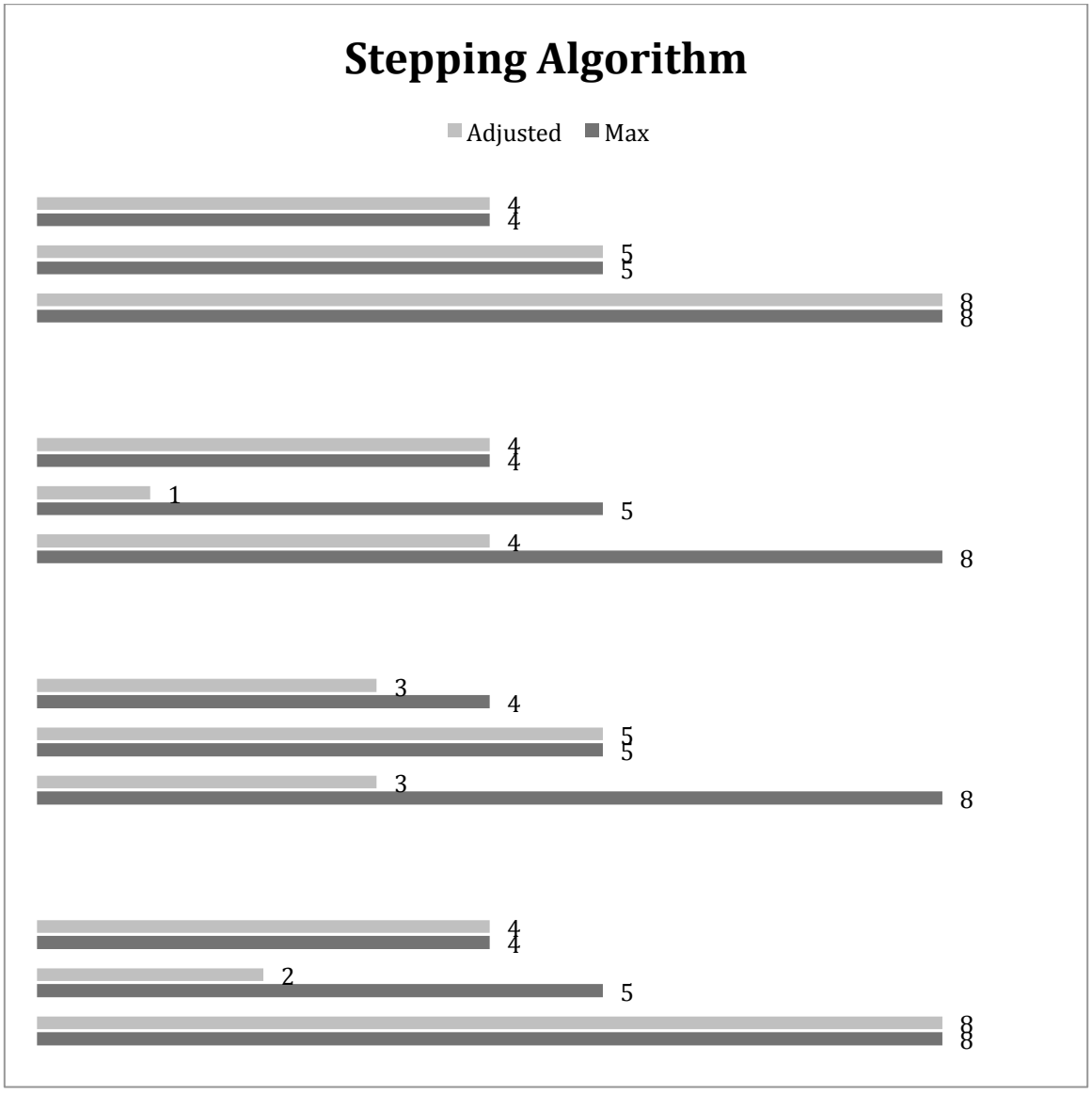

Figure 2 Example of Stepping Selection of 4 Steps with Respect to 3 Molecular Orbitals (assuming constant energy of incident particle). Notes on Step #1: MO1 is selected at step length of four; MO2 and MO3 are decremented by four. Notes on Step #2: MO1 was reset to step length of four after last step; MO2 is selected at step length of one; MO1 and MO3 are decremented by one. Notes on Step #3: MO2 was reset to step length of five. MO1 and MO3 are both selected at a step length of 3. MO2 is decremented by 3. Notes on Step #4: MO1 and MO3 are reset to their maximums after being selected by the previous step. MO2 is selected at the next step length at two.

2.5 Transport Algorithm

2.5.1 Force Field Map

The meshes containing the force fields are composed in a hierarchy of nested classes. The uppermost of which is the field map, which is assigned to each individual molecule and represents the bounding volume of the molecule. This class is a virtual (non-interacting) volume that contains both the gradient field for the incident particle (M_p) and the gradient field for the molecular electrons (M_o), which are overlapping but independent of each other. When the incident particle enters the field map, the field map navigates the incident particle through M_p and molecular electrons are "navigated" within M_o. The incident particle, however, operates on M_o. As the incident particle moves through M_p a full step length, it potentially traverses multiple volumes in M_p and M_o. When the incident particle reaches a boundary between mesh volumes in M_p or completes the full step, the perturbation on the field of M_o is calculated via:

$$F_{i,n+1} = F_{i,n} + k_e \frac{eQ_{e-}}{r_{12}^2} \vec{R}_{12} \tag{12}$$

where $F_{i,n+1}$ is the new gradient at iteration $n + 1$, Q_{e-} is the electron charge, e is the fundamental charge (keeping F_i scalable to charge), r_{12} is the distance between the incident particle and the mesh volume, and $\bar{R}_{12}$ is the normalized direction vector between the incident particle and the mesh volume.

The navigation of the incident particle is done classically, i.e. a step length is proposed and the particle moves according to the classical laws of motion. This method

represents a region of potential improvement, where the incident particle is treated quantum mechanically. If a molecular electron has already been ionized or excited to the anti-bonding orbital, the gradient field forces in M_p and M_o are rescaled to account for the missing molecular electron(s) (see *Forces on the Incident Particle* Section).

2.5.2 Treatment of Molecular Electric Field

Several algorithms underwent investigation for the best approach to solve the dynamics of the complex system. The key components that the final selected algorithm employs are:

1. Energy loss to the primary particle only via discrete physical events such as ionization, dissociate ionization (excitation to the anti-bonding orbital of water), and excitation
2. Conservation of the incident particle kinetic energy following a track without a discrete event

In order to address (1), the incident particle does not lose or gain energy through acceleration within the electric field of molecule. While this approach may appear to violate the known behavior of a charged particle in an electric field, the electric field of the molecule cannot be treated as a capacitor which remains insignificantly affected by a charge moving through its potential. Therefore, when the incident particle is interacting with the molecule, the incident particle is deflected within the electric field and the energy remains unchanged unless a discrete interaction occurs, e.g. ionization or excitation.

In order to address (2), an incident particle, which does not cause a discrete physical event such as excitation or ionization, does not shift the molecule to a different energy state of the molecule. Therefore the incident particle should not retain energy from the interaction and the incident particle should be treated as having elastically interacted with the molecule and return to the kinetic energy at the beginning of the interaction. Although rotational excitation and vibrational excitation from the incident particle is a legitimate cause of kinetic energy loss by the incident particle, molecular electronic state configurations are generalized by $\Delta E_{electronic} \gg \Delta E_{vibrational} \gg \Delta E_{rotational}$ and thus the energy losses via vibrational excitation and rotational excitation are relatively minor (although not entirely insignificant) and not currently accounted for in this early development of the full model.

2.5.3 Forces on the Incident Particle

The incident particle has two algorithmic situations in which it is subjected to Coulombic forces of the molecule: (1) incident particle is outside of the domain of the electron probability density mesh and (2) incident particle is inside the domain of the electron probability density mesh. In both cases, the Coulombic forces of the nuclei in a randomly selected position within one of the vibrational states are accounted for by randomizing the time state of the molecule at the creation of the incident particle. The molecule is held within this vibrational state due to an assumption that the time of the phase transition between vibrational states is much larger than the change in time during the interaction. The molecular nuclei are, however, moved within the vibrational state

slightly during transport to account for the dynamic nature of the vibration (although this position transition is largely negligible).

In the case of the incident particle outside of the domain of the electron probability density mesh, the Coulombic forces on the incident particle is computed via 4th order Runge-Kutta with a minimum of 50 different electron positions. In the case of the incident particle inside the domain of the electron probability density mesh, the Coulombic forces are a weighted average of the precompiled gradient map and the instantaneous electron positions derived from sampling with respect to their probabilities. The weighted average is defined by:

$$\vec{F}_{avg} = \frac{(N_T - 1) - N_{ionizations}}{N_T}\vec{F}_g + \frac{1}{N_T}\vec{F}_i + \vec{F}_{nuclei} \tag{13}$$

N_T is the maximum number of electrons in the molecule, $N_{ionizations}$ is the number of ionizations the molecule has previously undergone, $\vec{F}_g$ is the Coulombic force of the precompiled gradient field, $\vec{F}_i$ is the instantaneous Coulombic force of the molecular electrons in their currently sampled positions, and $\vec{F}_{nuclei}$ is the Coulombic forces of the nuclei. The weighting on the force, $\vec{F}_g$, is an approximation to account for changes in the gradient field value due to the missing electrons from ionization. Future development will have the molecular system transition to an electron probability distribution and gradient field corresponding to the molecule in the ionization state and also include models for electron capture, when the incident particle is an electron.

2.5.4 Mesh Boundary Detection

Transport through the mesh is handled with a boundary-crossing algorithm that uses three points on each of the six faces of each mesh volume, the starting point of the step, and the proposed ending point of the step extrapolated out from the starting point added to the scalar step length multiplied into the momentum direction of particle (see Figure 3). The boundary-crossing algorithm is defined by:

$$\begin{pmatrix} t \\ u \\ v \end{pmatrix} = \begin{pmatrix} x_a - x_b & x_1 - x_0 & x_2 - x_0 \\ y_a - y_b & y_1 - y_0 & y_2 - y_0 \\ z_a - z_b & z_1 - z_0 & z_2 - z_0 \end{pmatrix}^{-1} \begin{pmatrix} x_a - x_0 \\ y_a - y_0 \\ z_a - z_0 \end{pmatrix} \tag{14}$$

An intersection of the line with the plane between the point of x_a and x_b is defined when *t* is greater than zero and less than or equal to one.

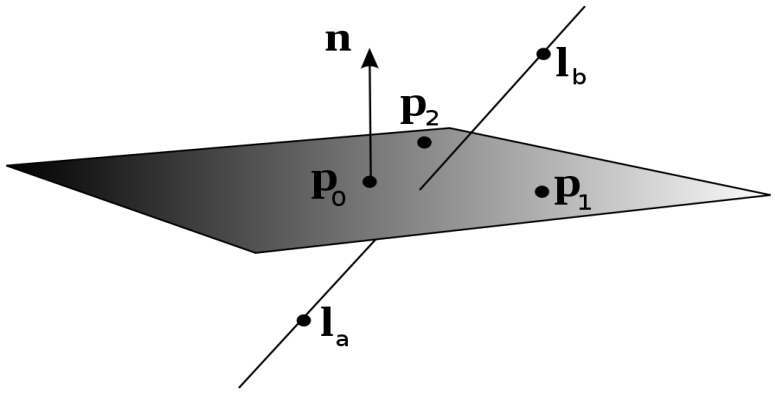

Figure 3 Graphical Depiction of Line-plane Intersection

2.6 Algorithm Description

In addition to the analysis of the results, this transport algorithm has the benefits of faster computation time and better elastics scattering than many of the other algorithmic considerations that have been tested in our work. The elastic scattering is derived from an approximation that arises from the assumption that the internal electric field of the molecule cannot be treated in the classical sense of a static electric field as found in a capacitor – an incident particle that is accelerated within the electric field of molecule does not undergo a change in total energy unless the molecule undergoes a discrete process such as an excitation or ionization. In other words, if an incident particle interacts with a molecule and does not cause a discrete process such as an excitation or ionization, the molecule should not impart or absorb any of its internal energy to the incident particle, as this would disrupt the equilibrium or ground state of the molecule that has the solution to many-body Schrödinger equation with specific molecular orbital kinetic energies and binding energies. In essence, the energy lost in the electromagnetic field of the particle is stored as potential energy in the particle and restored if the particle fails to cause a discrete process (elastically scatters).

The incident particle steps are treated as follows:

1. Compute step length of incident particle with respect to each orbital
2. Selected shortest adjusted step length (see *Stepping Algorithm* section)
3. Determine if the starting point is within the domain of the electron probability density mesh

   3.1. If outside domain → 4^{th} order Runge-Kutta

3.2. If inside domain → Use precompiled gradient maps and instantaneous positions

4. Step the incident particle

4.1. Reset the all the dynamic portions of molecular electron mesh to static values

4.2. Adjust the dynamic portion of the molecular electron gradient map by adding the perturbative force of the incident particle to the mesh volume and it's surrounding neighbors at each instance of crossing boundary into another mesh volume or at the conclusion of the step [number of surrounding neighbors is defined at runtime – standard setting is neighbors within 20 * average spacing between mesh volumes

4.3. Particle energy remains the same in principle, however, the velocity is adjusted due to acceleration (effectively storing kinetic energy as potential energy that is restored if the particle elastically scatters)

5. Calculate the excitation energies of the molecular electrons in the selected molecular orbital

5.1. Force under static conditions is computed via static gradient force of electron in pre-step sampled mesh volume + static gradient force of electron of post-step sampled mesh volume

5.2. Force under perturbed conditions is computed via dynamic gradient force of electron in pre-step sampled mesh volume + dynamic gradient force of electron in post-step sampled mesh volume

5.3. Excitation energy is defined as the dot product of [static force – dynamic force] and [post-step electron position – pre-step electron position]

5.4. The process is repeated several times with different samplings of electron positions (adjustable parameter set to 75 times – based on considerations of large set of sampled of electron positions and computation time). Excitation energy is the average of these excitation samples

6. Check the molecular electrons in the selected orbital for discrete physical events such as ionization and excitation

6.1. Ionization uses the final average excitation energy from all resamples

6.2. Excitation uses the final average of excitation energy from all resamples but can also use the list of running excitation energy averages of all the resamples

6.2.1. I.e. Each history represents the running average of excitation energies – the excitation energy history after 10 computations is the average of the first 10 computations.

6.2.2. This was used as an effort to simulate the transient properties of an excitation event since an excitation event must fit into a very small energy window

6.3. In the event of a ionization, conserve momentum between ejected electron and incident particle

6.4. In the event of an excitation, momentum is not conserved as experimental results suggest an excitation event does not alter the momentum of the incident particle (Champion, 2003)

2.7 Detailed Description of Discrete Processes

2.7.1 Excitation Energy of Molecular Electron

The excitation energy of the molecular electrons is determined during transport through the application of a method of molecular electronic field perturbation. The application of which seeks to ignore the instantaneous positions of the electrons with respect to the particle. The reasoning behind this paradigm is based on the wave nature of electron cloud. As previously stated, the perturbation of the incident particle is stored in a dynamic component of the electric field force vector of each mesh volume that is a sum of the perturbations in the molecular electric field from a history of incident particle positions. Labeling the dynamic component $\vec{F}_d$, and the static component $\vec{F}_s$, where the forces represent the sum of the dynamic and static force components of both the pre-step mesh volume and post-step mesh volume, the excitation energy is:

$$\Delta E_{excite} = (\vec{F}_d - \vec{F}_s) \bullet (\vec{X}_{post} - \vec{X}_{pre}) \tag{15}$$

where $\vec{X}_{post}$ is the post-step sampled position of the electron and $\vec{X}_{pre}$ is pre-step sampled position of the electron. In this method, a pseudo-path integral is evaluated over the step of the particle. Previous algorithm developments extended this path integral by segmenting this calculation to include computation of the dynamic minus static components in all intermediate mesh volumes between the pre-step and post-step mesh volumes, however, because of the significantly increased computational cost of this approach, mixed results, and deviation from the paradigm of wave-like treatment of the electrons in the electron cloud, this extra computation was excluded from our work.

2.7.2 Excitation

The definition of a molecular excitation is a process that modifies the internal state of the molecule without the emission of an electron. In particular these process are electronic transitions towards Rydberg or degenerate states, dissociative attachment leading to the formation of negative ions, dissociative excitation leading to the formation of excited radicals, and vibrational and rotational excitation. The contribution of all these processes is non-negligible in the energy deposition of the incident particle.

Our excitation algorithm is divided into two categories: (1) promotion of a molecular electron to an occupied orbital, and (2) promotion of a molecular electron to the lowest unoccupied molecular orbital (LUMO) of the water molecule in the ground state which is assumed to cause dissociative excitation and leads to the formation of radicals (Elles, Shkrob, Crowell, & Bradforth, 2007). Vibrational and rotational excitation, and dissociative attachment are not included in the current model. Transition to the Rydberg and degenerate states could in theory be derived from our current model but is outside the detail of our excitation algorithm. The cross sections derived from (1) can be verified by empirical data of characteristic X-rays. The cross section derived from (2) will be used in the future to validate our model with G-values associated with radical production in the radiolysis of water.

The method of determining an excitation is as follows: After the molecular electrons within the molecular orbital selected by the stepping algorithm have computed their excitation energy, the algorithm begins by determining which energy window between higher occupied orbitals the excitation energy can fit within. Once the available

transition(s) are determined, the difference between of the excitation energy and the transition energy is computed to determine whether or not the excitation energy has the appropriate amount of energy to make the transition. The determining factor of this transition is an arbitrary simple percent difference parameter ε of which the default is 0.05% according to:

$$\frac{|E_e - E_T|}{E_T} < \varepsilon \tag{16}$$

where E_e is the excitation energy and E_T is the transition energy window. An excitation is tallied according to which orbital the electron originated from and which orbital the electron was promoted to and the transition energy of the de-excitation photon is saved. The methodology allows for future analysis of excitation cross-sections between specific shells.

The algorithm for excitation to the lowest unoccupied molecular orbital, which is assumed as the cause of dissociative excitation, follows the same algorithm as a standard excitation with one minor alteration. This alteration is the molecular electron is no longer valid for the remainder of the incident particle track. In other words, the electron is not de-excited back to the original orbital. This is due to an assumption that once the particle has been promoted to this orbital, the molecule begins to dissociate and the state of the molecule has been permanently changed. The molecular electrons occupying the outermost orbitals of the molecule are dropped down to fill the inner shell vacancy left by the promotion to the anti-bonding orbital – i.e. the Auger effect.

2.7.3 Ionization

Ionization is the dominant electromagnetic component of energy loss above ~50 eV (Champion, 2003) and relevant down to energies of ~9-10 eV as the minimum ionization potential from GAUSSIAN calculations is 8.88 eV. One of the primary goals of our model is to develop accurate predictions of the kinetic energy associated with the secondary electrons cross sections in addition to cross sections for ionizations.

The ionization algorithm is as follows: After the molecular electrons within the molecular orbitals selected by the stepping algorithm have computed their excitation energy, the algorithm begins by determining the amount of energy required to ionized the electron (i.e. ionization potential), which is defined by the absolute value of the binding energy. The excitation energy is compared against the ionization potential and in the event the excitation energy exceeds the binding energy, the electron is determined as ionized and the molecular electron is no longer valid for the remainder of the incident particle interaction with the molecule. The secondary electron kinetic energy is determined as the excitation energy minus the binding energy. The incident particle undergoes momentum conservation with the ionized molecular electron. The initial momentum direction of the ionized molecular electron is not assumed to be isotropic but defined as the momentum direction from the previously sampled electron position to the most recently sampled electron position. Analysis of the distribution of secondary electron momentum directions has not been done and future analysis may alter this assumption. The momentum conservation of the molecular electron is defined as:

$$\vec{v}_2^{'} = \frac{m_1\vec{v}_1 + m_2\vec{v}_2 - m_1\vec{v}_1^{'}}{m_2} \tag{17}$$

where the subscript 2 is the molecular electron, the subscript 1 is the incident particle, m is the mass of the particle, and $\vec{v}$ is the velocity of the particle. The incident particle momentum conservation is defined as:

$$\vec{v}_1^{'} = \frac{m_1\vec{v}_1 + m_2\vec{v}_2 - m_2\vec{v}_2^{'}}{m_1} \tag{18}$$

where the subscript 1 is the incident particle, the subscript 2 is the molecular electron, m is the mass of the particle, and $\vec{v}$ is the velocity of the particle. The scalar value of the velocity with respect to the incident particle is computed via $\sqrt{\frac{2E}{m}}$ where E represents the kinetic energy of the incident particle and m is the mass of the incident particle. The kinetic energy of the incident particle is taken as the original kinetic energy not accounting for change in kinetic energy from acceleration in the electric field of the particle, i.e. the kinetic energy that is the summation of the kinetic energy accounting for acceleration of the incident particle in the electric field plus the potential energy that is gained or lost from acceleration in the electric field of the molecule.

In the event of an ionization of a molecular electron from an inner-shell, the molecular electrons in the molecular orbitals comprising the outermost molecular orbital are dropped down to fill the inner shell vacancy – i.e. the Auger effect.

3. RESULTS

3.1 Computational Requirements

The computational power required for these results is not insignificant. Multi-threading efforts failed to decrease computation time as the components of this system are intricately interwoven. Parallelism with MPI is a future development not yet completed. The compiled results required four days of computation time and are a combination of four separate simulations on independent cores with differing initial random number seeds. The code was written in C++ and relies heavily on C++11 and works with GNU GCC 4.7 and Clang 4.1. The random number generator is the STL default random engine included in the C++11 extension to the C++ language. Due to high usage of the random number generator, the random seed is reset every 100 incident particles and excluded from using any random seed previously utilized. Memory requirements can reach 2 GB at the end of the simulation although no memory leaks were detected during profiling. The application requires the installation of the CLHEP library (Class Library for High Energy Physics, CERN) and is complete with OpenGL and SILO data format (Lawrence Livermore National Laboratory) visualization.

3.2 Known Shortcomings and Deficiencies

The largest shortcoming is the construction of the system. The electron probability densities of the molecular orbitals were corrected for the liquid state; however, the representation of a single molecule implies that the water molecule and interacting particle are in an isolated system. In reality, the density of water suggests that the

starting point of the particle (~3.2 Å from origin) is relatively close to the center of another water molecule. However, the full electron probability distribution is seen in Figure 4 and 5 and the geometrical configuration cannot be reduced. Additionally to improve computational time, symmetry should be employed when selecting the angle of incidence on the water molecule and especially for more complex molecules whose computation time will be inherently extended.

The entire project included approximately 150 classes and was in excess of 35,000 lines of code. The entirety of the code has been written from scratch and has been a very significant undertaking in the timeframe of approximately 9 months. While the algorithms have been verified as much as possible, the code is not devoid of minor bugs and therefore the conclusions drawn from the results are preliminarily interpreted. The primary improvement that needs to be made is a unified simplification of the algorithms described in the code.

3.3 Benchmarking

The main focus of our benchmarking was to determine whether our approach could produce stopping powers for incident electrons interacting with water molecules consistent with stopping power approximations from a mainstream Monte-Carlo code capable of transporting down to the energy ranges of interest. The Monte Carlo code chosen for comparison was Geant4-DNA (Chauvie, et al., 2006), which includes physics models for electrons in water down to the eV range (implementation of Champion, 2003). Geant4-DNA has elastic scattering models from 0 eV to 1 MeV (cutoff is 7.4 eV), electronic excitation models from 9 eV to 1 MeV, ionization models from 11 eV to

1 MeV, vibrational excitation from 2 eV to 100 eV and electron attachment from 4 eV to 13 eV. In addition to comparison of stopping powers, ionization to excitation ratios and average secondary electron energies were also considered over a range of 4 eV to 1 keV. While the ultimate goal is to develop a valid transport model for molecules other than water, the application of our model to the water molecule was the crucial starting point in determining the validity of our paradigm.

3.3.1 Geant4-DNA Model

The Geant4-DNA model used Geant4.9.6.1 (Agostinelli, et al., 2003). The geometry was a 1-meter cube of the material "G4_WATER" constructed with G4NistManager at standard density and utilized a step limiter of 0.5 nanometers within this volume. The physics of the Geant4-DNA model, which are an implementation of the methodology developed by Champion (2003), utilized the G4DNA modular physics constructor, G4EmDNAPhysics, with the additional electromagnetic process options of:

- SetAuger(ON = true)
- SetFluo(ON = true)
- SetIntegral(ON = true)
- SetLossFluctuations(ON = true)
- SetLPMFlag(ON = true)
- SetMscLateralDisplacement(ON = true)
- SetPIXE(ON = true)
- SetRandomStep(ON = true)

- SetSplineFlag(ON = true)

defined in the G4EmProcessOptions class of Geant4. The default cut for electrons, positrons, gammas, and protons (cut is a term in Geant4 that is defined as the minimum distance a secondary particle must be able to travel in order to be created and subsequently transported in the simulation) were 1 nanometer. The energy range of the production cuts table was also set (the energy-wise alternative to setting a cut) was 0.1 eV to 1 GeV. The primary particles were electrons centered at the origin with isotropic initial momentum direction and distributed linearly of the energy range of 5 eV to 1 keV. The detailed description of the materials and physics is provided in the Appendix.

3.3.2 Linear Energy Loss

The linear energy loss comparison (see Figure 4) makes similar predictions to Geant4-DNA with the exception of the energy range between 10 eV and 40 eV. In the energy range of 10 eV to 40 eV, MCMT predicts a local maximum of energy loss while Geant4-DNA predicts a local minimum. However, this local minimum in Geant4-DNA is not seen until a very large number of particles have been simulated in Geant4 and until that point, a local maximum similar to MCMT can be found. Although cross-sections have not been generated, the relative agreement of linear energy loss can be preliminarily interpreted as a relative agreement between total inelastic cross sections.

However, this is not the entire story. An alternative algorithm provides linear energy loss values about 50% lower than the presented MCMT algorithm above about 50 eV. This alternative algorithm may prove to be significant because an incident particle will

be simultaneously interacting with multiple molecules given that the true state of the particle-molecule interaction is not an isolated system (the only modification in this alternative algorithm was the inclusion of resetting the dynamic components of the mesh volumes at the beginning of each step). The multiple molecule interaction may compensate for the discrepancies between linear energy loss with Geant4-DNA and linear energy loss with MCMT.

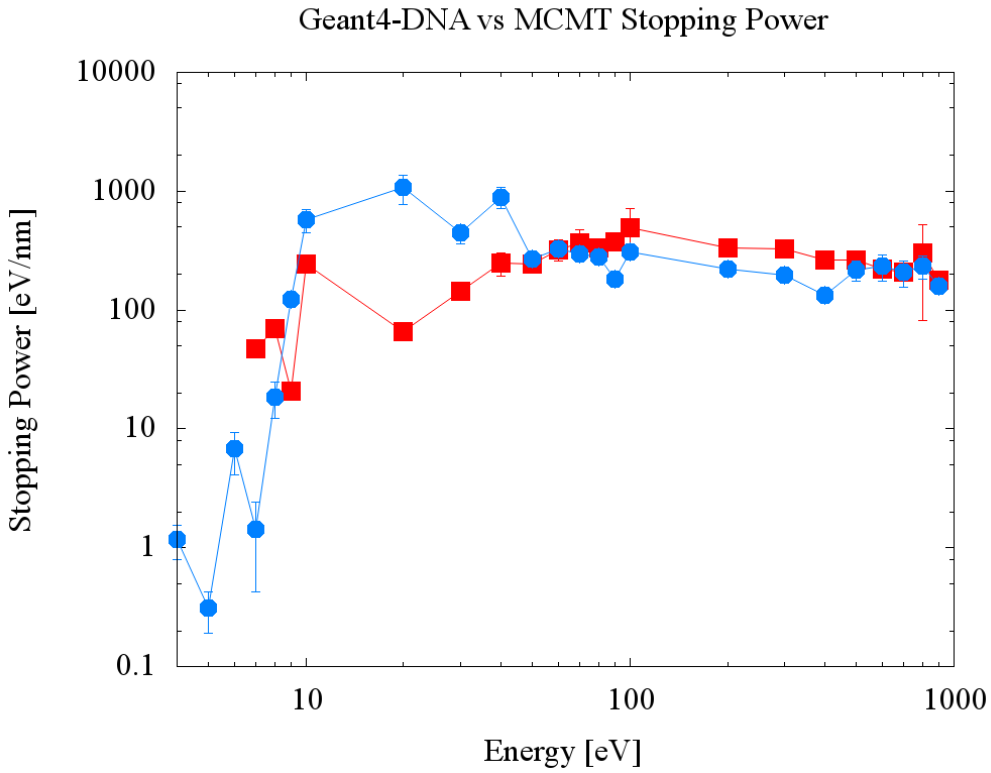

Figure 4 Comparison of Linear Energy Loss [2σ]. Filled squares represent Geant4-DNA; filled circles represent MCMT. In the energy range between 10 eV and 40 eV, there are significant discrepancies between MCMT and Geant4-DNA. The local minimum seen in Geant4-DNA, in contrast to the local maximum seen in MCMT, does not appear until a large sampling of particles has been done in Geant4-DNA.

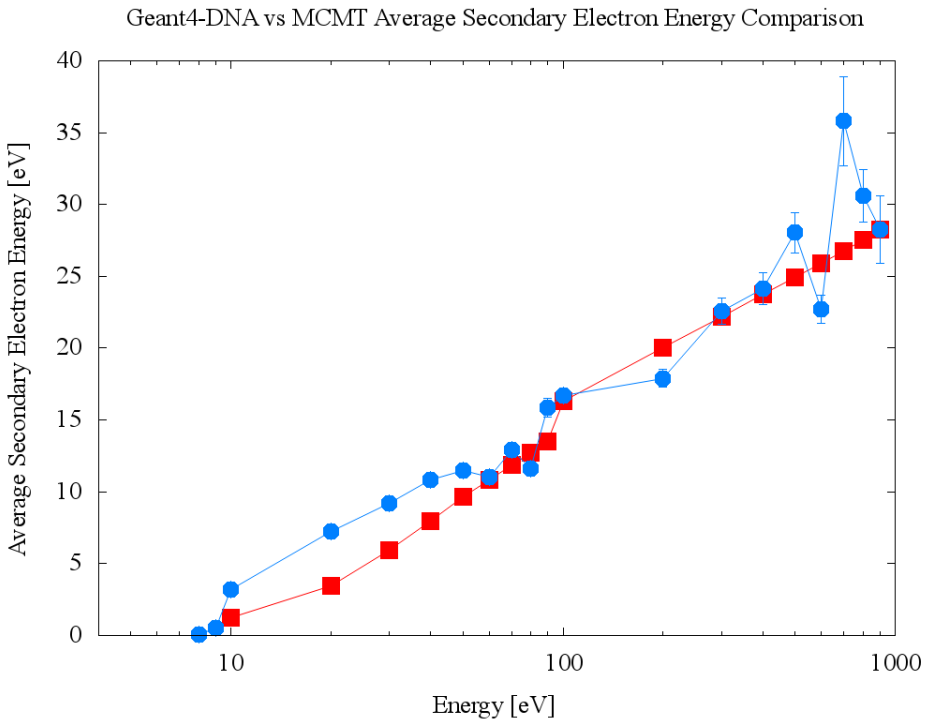

Figure 5 Comparison of Secondary Electron Energies [2σ]. Filled squares represent Geant4-DNA; filled circles represent MCMT. In the energy range above 500 eV, there are significant discrepancies between MCMT and Geant4-DNA. These fluctuations in MCMT are under investigation and may simply be an artifact of too little sampling in the energy range.

3.3.3 Secondary Electron Energies

The most consistent data between Geant4-DNA and MCMT is the secondary electron energies over almost the entire energy range of 10 eV to 1 keV (see Figure 5). In general, the secondary electrons energies predicted by MCMT are larger than Geant4-DNA although this difference is relatively small compared with the discrepancies in other benchmarked data. The largest energy range of deviation from Geant4-DNA is

above 50 keV, however, this energy range received a lower number of incident particle as our primary interest was the comparison as very low incident electron energies.

3.3.4 Ionization/Excitation Ratios

The most inconsistent data between Geant4-DNA and MCMT is the ionization to excitation ratios (see Figure 6). However, this data is very difficult to converge in MCMT as this ratio is highly dependent on the number of excitations, which is a consequence of a three-fold issue. The first issue is the incomplete modeling of excitations – MCMT does not do extensive analysis on the different types of excitations previously described in Section 2.7.2. The second issue is the intrinsic statistical nature of the Monte Carlo method. Since MCMT is a Monte Carlo method and the relative number of excitations compared to ionizations is generally small, a small difference in the number of excitations cause a large difference in the resulting ratio. A larger sampling of incident particle energies and initial momentum directions will likely produce more discernable conclusions but this is difficult given the amount of computational resources currently required. The third and final issue is the arbitrary window parameter ε that has a default value of 0.05%. This value may in fact be too tight and is addressed later on in the *Discussion and Future Work* section.

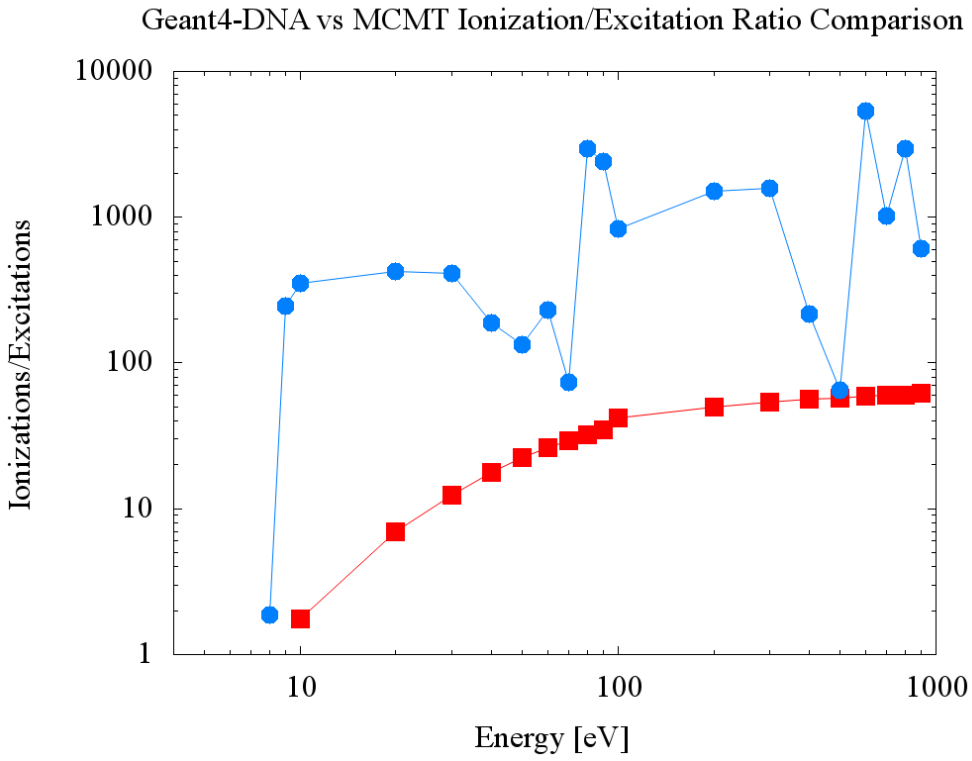

Figure 6 Comparison of Ionization/Excitation Ratios. Filled squares represent Geant4-DNA; filled circles represent MCMT. Statistical uncertainty was not computed.

4. DISCUSSION AND FUTURE WORK

The beauty of our approach is the fundamental treatment of the molecule. While the current methodology has various algorithm settings, our paradigm, when fully developed, will require no vapor-to-liquid density scaling, adjustable parameters, or empirical data fitting and will be capable of being applied to any molecule. Our methodology is rooted in the solution to the many-body Schrödinger equation and with access to an application capable of solving this equation, of which there are many both freely and commercially available, GAUSSIAN, GAMESS-US, NWChem, etc., the low-energy cross sections for any molecule can be determined and utilized in any condensed history Monte Carlo particle transport code of choice.

The shortcoming of the previous approaches in the low-energy regime lies in the treatment of the water molecule itself – the interaction of an incident charged particle with an atom or molecule with comparable kinetic energies of the incident particle and molecular orbitals should not be treated as a point-wise potential. At low kinetic energies, the incident particle has a non-insignificant interaction time with the electron probability distribution – analogous to a stationary charge being subjected to a varying electric potential as the nuclei cycle through their vibrational modes. A molecule at the bottom of the potential energy well wants to remain as close to the minimum as possible and this state is achieved by the electron probability distributions solvable via the many-body Schrödinger equation. The presence of an extraneous charged particle, causes a disruption in the molecule's equilibrium configuration and produces a shift up of the potential energy well – much as a balloon resists the injection of air during inflation in

conjunction with expanding to accommodate the extra air, the molecular system resist the injection of the charged particle (an electron in this analogy) by reconfiguring the electron probability distribution in order to accommodate the excess charge. In developing our paradigm, it was found the treatment of the molecular electrons as a probability distribution produced better results than those computed by Coulombic forces from the electrons at discrete positions. The difficulty in simulating this approach lies in the wave portion of the sub-atomic particles. The response of the incident particle and molecular nuclei were treated classically and therefore subject to Newton's 1st and 3rd laws of motion. The wave-like properties of the electron probability distribution are a source of significant computational resources in the approach and further development of the methodology must not only achieve accuracy in its predictions but also reduce the computational requirements.

The MCMT paradigm of the combination of quantum mechanical molecular descriptions and classical transport appears to have merit based on our comparison with Geant4-DNA. However, there remains much more to be done to prove the validity of the model. The following extensions need to be included:

- Include additional physics processes
    - Vibrational excitation and attachment (e-)
    - Electron capture (protons)
    - Charge transfer (baryons, e.g. proton, H, C, N, O, Fe)
- Compare results with additional Monte Carlo codes and experimental data

- Compare G-value predictions for radical production
- Benchmark MCMT with Geant4-DNA for incident protons, hydrogen, alpha particles, alpha+ particles (He^{-}), helium, carbon, nitrogen, oxygen, and iron
- Test with larger molecules
    - This has been done with adenine but benchmarking data as not been found
- Evaluate the window fitting parameter for determining excitations
    - This may include a significant adjustment to the excitation algorithm as the excitation process is studied and subsequently modeled in greater detail.
- Analyze results between different computational chemistry levels of theory and basis sets – See Tables 4 and 5 (Sholl & Steckel, 2009)

Table 4 Computed Properties of CH_4 Molecule for Four Levels of Theory using pVTZ Basis Set [a]

Level of Theory	C—H (Å)	% Error	Ionization (eV)	% Error	Relative Time
HF[b]	1.085	-0.8	11.49	-8.9	1
DFT (B3LYP)	1.088	-0.5	12.46	-1.2	1
MP2[c]	1.085	-0.8	12.58	-0.2	2
CCSD[d]	1.088	-0.5	12.54	-0.5	18

[a] Errors are defined relative to the experimental value
[b] Hartree-Fock
[c] Møller–Plesset perturbation theory
[d] Couple-cluster Standard

Table 5 Properties of CH_4 Calculated Using DFT (B3LYP) with Four Different Basis Sets [a]

Basis Set	Number of Basis Functions	C—H (Å)	% Error	Ionization (eV)	% Error	Relative Time
STO-3G	27	1.097	0.3	12.08	-4.2	1
cc-pVDZ	61	1.100	0.6	12.34	-2.2	1
cc-pVTZ	121	1.088	-0.5	12.46	-1.2	2
cc-pVQZ	240	1.088	-0.5	12.46	-1.2	13

[a] Errors are defined relative to the experimental value. Time is defined relative to STO-3G calculations

Additionally, a correction needs to be applied to the perturbed component of M_o (see *Treatment of Molecule Electric Field* section). The incident particle and molecular electrons are stepped with respect to each other, thus, the pre-step sampled electron is operated on by the perturbed force field of M_o at the pre-step position of incident particle (defined as the incident particle position when it was last stepped with respect to that specific molecular orbital) and the post-step sampled electron is operated on by the perturbed force field of M_o at the post-step position of the incident particle (defined as the current incident particle position). As such, the perturbed force field M_o must reflect the conditions at these instances in time instead of always reflecting the perturbed conditions at the incident particle current position. This would require a slight alteration of the computation of $\vec{F}_d$ (see *Excitation of Molecular Electrons* section) yet to be defined.

The implications of this methodology are significant. With the aforementioned corrections and enhancements, this methodology could be applied to any molecule with almost zero correction parameters and completely remove the need for the principle of superposition. This would have a significant impact on radiobiology simulations by enabling a greater understanding of the microscopic biological effect of charged particle irradiation.

5. CONCLUSIONS

The present paper presents our work on a transport method for determining the inelastic electromagnetic interactions between an incident charged particle and a given molecule, which we are calling Monte Carlo Molecular Transport (MCMT). Our present work is limited to incident electrons over an energy range of 5 eV to 1 keV and the water molecule. The calculations from our work for linear energy loss, ionization to excitation ratio, and secondary electron kinetic energies have been compared to Geant4-DNA using Geant4.9.6.1 with reasonable agreement for linear energy loss and secondary electron energies. However, there is significant deviation in the ionization to excitation ratio predictions. The cross sections for these inelastic processes were not computed but the reasonable agreement of linear energy loss between MCMT and Geant4-DNA indicates agreement in the total inelastic cross section.

Due to the nature of statistical convergence in our Monte Carlo method and the wide range of incident particle energies, scattering cross sections have not been analyzed because these cross sections need to be converged not only for energy but also for the range of scattering angles.

Additionally, our fundamental and detailed treatment of the molecule provides an excellent framework for the computation of the interaction cross sections. While further refinement of the methodology is needed for more accurate results, the framework can provide eight-fold differential cross sections – i.e. cross sections with respect to the angle of incidence of the incident particle (φ and θ), orientation of the molecule (Euler

angles α, β, and γ), energy of the incident particle (E_i), and molecular orbital (N_{MO}) – which will allow detailed studies of the kinematics of the electromagnetic interaction. Moreover, the algorithm can be applied on a per-molecule basis. This will allow the production of the low-energy cross sections for each component of a microscopically heterogeneous system and thereby replace the use of the principle of superposition. The removal of the principle of superposition will further enhance the ability to accurately simulate and study the interaction of charged particles in these microscopically heterogeneous systems such as a cell nucleus.

REFERENCES

Agostinelli, S., Allison, J., Amako, K., Apostolakis, J., Araujo, H., Arce, P., et al. (2003). Geant4—a simulation toolkit. *Nuclear Instruments and Methods in Physics Research Section A: Accelerators, Spectrometers, Detectors and Associated Equipment , 506* (3), 250-303.

Becke, A. D. (1988). Density-functional exchange energy approximation with correct asymptotic behavior. *Physical Review A , 38* (6), 3098-3100.

Boudaïffa, B., Cloutier, P., Hunting, D., Huels, M. A., & Sanche, L. (2002). Cross Sections for Low-Energy (10−50 eV) Electron Damage to DNA. *Radiation Research , 157* (3).

Champion, C. (2003). Theoretical cross sections for electron collisions in water: structure of electron tracks. *Physics in Medicine and Biology , 48*, 2147-2168.

Champion, C., Hanssen, J., & Hervieux, P. A. (2002). Electron impact ionization of water molecule. *Journal of Chemical Physics , 117*, 197-204.

Champion, C., Hanssen, J., & Hervieux, P. A. (2001). Influence of molecular orientation on the multiple differential cross sections for the (e,2e) process on a water molecule. *Physical Review A , 63*.

Chan, A. C. (2007). *Distored Wave Born Approximation For Inelastic Atomic Collision.* University of Waterloo, Department of Mathematics. Ontario, Canada: University of Waterloo.

Chauvie, S., Francis, Z., Guatelli, S., Incerti, S., Mascialino, B., Montarou, G., et al. (2006). Monte Carlo simulation of interactions of radiation with biological systems at the cellular and DNA levels : The Geant4-DNA Project,. *Radiation Research , 166* (4), 652-689.

Deutsch, H., Becker, K., Matt, S., & Mark, T. D. (1999). Theoretical Determination of absolute electron-impact ionization cross sections of molecules. *International Journal of Mass Spectrometry , 111* (5), 1964.

Elles, C. G., Shkrob, I. A., Crowell, R. A., & Bradforth, S. E. (2007). Excited state dynamics of liquid water: Insight from the dissociation reaction following two-photon excitation. *Journal of Chemical Physics , 126* (16).

Friedland, W., Dingfelder, M., Kundrat, P., & Jaboc, P. (2011). Track structures, DNA targets and radiation effects in the biophysical Monte Carlo simulation code PARTRAC. *Mutation Research , 711* (1-2), 28-40.

Frisch, M. J., Trucks, G. W., Schlegel, H. B., Scuseria, G. E., Robb, M. A., Cheeseman, J. R., et al. (2009). GAUSSIAN, Rev A.1. Wallingford, CT: GAUSSIAN, Inc.

Huang, W., Kim, Y.-K., & Rudd, M. E. (1996). New Model for Electron-Impact Ionization Cross Section of Molecules. *Journal of Chemical Physics , 104* (8).

Irikura, Y.-K. K., & Karl, K. (2000). Electron-Impact Ionization Cross Sections for Polyatomic Molecules, Radicals, and Ions. (K. L. K. A. Berrington, Ed.) *AIP Conference Proceedings , 543* (1), 220.

Lee, C., Yang, W., & Parr, R. G. (1988). Development of the Colle-Salvetti correlation-energy formula into a functional of the electron density. *Physical Review B , 37* (2), 785-789.

Pimblott, S. M., & LaVerne, J. A. (2007). Production of low-energy electrons by ionizing radiation. *Radiation Physics and Chemistry , 76* (8-9), 1244-1247.

Seo, H., Pia, M. G., Saracco, P., & Kim, C.-H. (2010). Design, development and validation of electron ionisation models for nan-scale simulation. *Joint International Conference on Supercomputing in Nuclear Applications and Monte Carlo.* Tokyo.

Sholl, D. S., & Steckel, J. A. (2009). *Density Functional Theory: A Practical Introduction.* Hoboken, NJ: John Wiley & Sons, Inc.

Tomasi, J., Mennuci, B., & Cammi, R. (2005). Quantum Mechanical Continuum Solvation Models. *Chemical Review , 105*, 2999-3093.

Woon, D. E., & Dunning, Jr., T. H. (1995). Gaussian basis sets for use in correlated molecular calculations. V. Core-valence basis sets for boron through neon. *Journal of Chemical Physics , 103* (11), 4572-4585.

APPENDIX

```
***** TABLE : NB OF MATERIALS = 1 *****

MATERIAL: G4_WATER H_2O     DENSITY:  1.000 G/CM3     RADL:  36.083 CM
NUCL.INT.LENGTH:  75.517 CM  IMEAN:  78.000 EV
 ---> ELEMENT: H (H)  Z =  1.0  N =  1.0  A =  1.01 G/MOLE
    ---> ISOTOPE:  H1  Z =  1  N =  1  A =  1.01 G/MOLE  ABUNDANCE:  99.99 %
    ---> ISOTOPE:  H2  Z =  1  N =  2  A =  2.01 G/MOLE  ABUNDANCE:  0.01 %
     ELMMASSFRACTION:  11.19 %  ELMABUNDANCE  66.67 %

 ---> ELEMENT: O (O)  Z =  8.0  N =  16.0  A =  16.00 G/MOLE
    ---> ISOTOPE:  O16  Z =  8  N =  16  A =  15.99 G/MOLE  ABUNDANCE:  99.76 %
    ---> ISOTOPE:  O17  Z =  8  N =  17  A =  17.00 G/MOLE  ABUNDANCE:  0.04 %
    ---> ISOTOPE:  O18  Z =  8  N =  18  A =  18.00 G/MOLE  ABUNDANCE:  0.20 %
     ELMMASSFRACTION:  88.81 %  ELMABUNDANCE  33.33 %

PHOT:  FOR GAMMA  SUBTYPE= 12
   LAMBDAPRIME TABLE FROM 200 KEV TO 10 TEV IN 54 BINS
   ======  EM  MODELS  FOR  THE  G4REGION    DEFAULTREGIONFORTHEWORLD
======
LIVERMOREPHELECTRIC :  EMIN=          0  EV      EMAX=          1  GEV
ANGULARGENSAUTERGAVRILA  FLUOACTIVE
   PHOTOELECTRIC :  EMIN=          1  GEV      EMAX=          10  TEV
ANGULARGENSAUTERGAVRILA  FLUOACTIVE

COMPT:  FOR GAMMA  SUBTYPE= 13
   LAMBDA TABLE FROM 100 EV  TO 1 MEV IN 28 BINS, SPLINE: 1
   LAMBDAPRIME TABLE FROM 1 MEV TO 10 TEV IN 49 BINS
   ======  EM  MODELS  FOR  THE  G4REGION    DEFAULTREGIONFORTHEWORLD
======
  LIVERMORECOMPTON :  EMIN=      0 EV   EMAX=      1 GEV  FLUOACTIVE
    KLEIN-NISHINA :  EMIN=      1 GEV   EMAX=      10 TEV

CONV:  FOR GAMMA  SUBTYPE= 14
   LAMBDA TABLE FROM 1.022 MEV TO 10 TEV IN 49 BINS, SPLINE: 1
   ======  EM  MODELS  FOR  THE  G4REGION    DEFAULTREGIONFORTHEWORLD
======
 LIVERMORECONVERSION :  EMIN=      0 EV   EMAX=      1 GEV
     BETHEHEITLER :  EMIN=      1 GEV   EMAX=      80 GEV
   BETHEHEITLERLPM :  EMIN=      80 GEV   EMAX=      10 TEV

RAYL:  FOR GAMMA  SUBTYPE= 11
   LAMBDA TABLE FROM 100 EV  TO 100 KEV IN 21 BINS, SPLINE: 0
```

```
   LambdaPrime table from 100 keV to 10 TeV in 56 bins
   ===== EM models for the G4Region DefaultRegionForTheWorld
======
  LivermoreRayleigh : Emin=      0 eV   Emax=      1 GeV   CullenGenerator
  LivermoreRayleigh : Emin=      1 GeV   Emax=     10 TeV   CullenGenerator

e-_G4DNAElastic: for e-  SubType= 51
 Total cross sections computed from DNAChampionElasticModel model
   ===== EM models for the G4Region DefaultRegionForTheWorld
======
DNAChampionElasticModel : Emin=      0 eV   Emax=      1 MeV

e-_G4DNAExcitation: for e-  SubType= 52
 Total cross sections computed from DNABornExcitationModel
   ===== EM models for the G4Region DefaultRegionForTheWorld
======
DNABornExcitationModel : Emin=      0 eV   Emax=      1 MeV

e-_G4DNAIonisation: for e-  SubType= 53
 Total cross sections computed from DNABornIonisationModel
   ===== EM models for the G4Region DefaultRegionForTheWorld
======
DNABornIonisationModel : Emin=      0 eV   Emax=      1 MeV  FluoActive

e-_G4DNAVibExcitation: for e-  SubType= 54
 Total cross sections computed from DNASancheExcitationModel
   ===== EM models for the G4Region DefaultRegionForTheWorld
======
DNASancheExcitationModel : Emin=      0 eV   Emax=     100 eV

e-_G4DNAAttachment: for e-  SubType= 55
 Total cross sections computed from DNAMeltonAttachmentModel
   ===== EM models for the G4Region DefaultRegionForTheWorld
======
DNAMeltonAttachmentModel : Emin=      0 eV   Emax=     13 eV

msc: for e+  SubType= 10
   RangeFactor= 0.04, stepLimitType: 2, latDisplacement: 1, skin= 1,
geomFactor= 2.5
   ===== EM models for the G4Region DefaultRegionForTheWorld
======
     UrbanMsc95 : Emin=      0 eV   Emax=     10 TeV  Table with 77 bins Emin=
100 eV   Emax=    10 TeV
```

```
### === Deexcitation model UAtomDeexcitation is activated for 1 region:
      DefaultRegionForTheWorld

### === G4UAtomicDeexcitation::InitialiseForNewRun()
### === PIXE model for hadrons: Empirical 1
### === PIXE model for e+-:    Livermore 1

eIoni:  for e+  SubType= 2
   dE/dx and range tables from 100 eV  to 10 TeV in 77 bins
   Lambda tables from threshold to 10 TeV in 77 bins, spline: 1
   finalRange(mm)=  0.1,  dRoverRange=  0.2,  integral:  1,  fluct:  1,
linLossLimit= 0.01
   =====  EM  models  for  the  G4Region    DefaultRegionForTheWorld
======
    MollerBhabha :  Emin=      0 eV   Emax=      10 TeV
   CSDA range table up to 1 GeV in 35 bins

eBrem:  for e+  SubType= 3
   dE/dx and range tables from 100 eV  to 10 TeV in 77 bins
   Lambda tables from threshold to 10 TeV in 77 bins, spline: 1
   LPM flag: 1 for E > 1 GeV
   =====  EM  models  for  the  G4Region    DefaultRegionForTheWorld
======
       eBremSB :  Emin=      0 eV   Emax=      1 GeV  DipBustGen
       eBremLPM :  Emin=      1 GeV  Emax=      10 TeV  DipBustGen

annihil:  for e+  SubType= 5
   =====  EM  models  for  the  G4Region    DefaultRegionForTheWorld
======
      eplus2gg :  Emin=      0 eV   Emax=      10 TeV

proton_G4DNAExcitation:  for proton  SubType= 52
 Total cross sections computed from DNAMillerGreenExcitationModel and
DNABornExcitationModel models
   =====  EM  models  for  the  G4Region    DefaultRegionForTheWorld
======
DNAMillerGreenExcitationModel :  Emin=      0 eV   Emax=      500 keV
DNABornExcitationModel :  Emin=      500 keV  Emax=      100 MeV

proton_G4DNAIonisation:  for proton  SubType= 53
 Total  cross  sections  computed  from  DNARuddIonisationModel  and
DNABornIonisationModel models
   =====  EM  models  for  the  G4Region    DefaultRegionForTheWorld
======
```

DNARuddIonisationModel : Emin= 0 eV Emax= 500 keV FluoActive
DNABornIonisationModel : Emin= 500 keV Emax= 100 MeV FluoActive

proton_G4DNAChargeDecrease: for proton SubType= 56
Total cross sections computed from DNADingfelderChargeDecreaseModel model
===== EM models for the G4Region DefaultRegionForTheWorld ======
DNADingfelderChargeDecreaseModel : Emin= 0 eV Emax= 100 MeV

alpha_G4DNAExcitation: for alpha SubType= 52
Total cross sections computed from DNAMillerGreenExcitationModel
===== EM models for the G4Region DefaultRegionForTheWorld ======
DNAMillerGreenExcitationModel : Emin= 0 eV Emax= 400 MeV

alpha_G4DNAIonisation: for alpha SubType= 53
Total cross sections computed from DNARuddIonisationModel
===== EM models for the G4Region DefaultRegionForTheWorld ======
DNARuddIonisationModel : Emin= 0 eV Emax= 400 MeV FluoActive

alpha_G4DNAChargeDecrease: for alpha SubType= 56
Total cross sections computed from DNADingfelderChargeDecreaseModel model
===== EM models for the G4Region DefaultRegionForTheWorld ======
DNADingfelderChargeDecreaseModel : Emin= 0 eV Emax= 400 MeV

Region <DefaultRegionForTheWorld> -- -- appears in <World> world volume
This region is in the mass world.
Root logical volume(s) : World
Pointers : G4VUserRegionInformation[0], G4UserLimits[0], G4FastSimulationManager[0], G4UserSteppingAction[0]
Materials : G4_WATER
Production cuts : gamma 1 nm e- 1 nm e+ 1 nm proton 1 mm

Region <DefaultRegionForParallelWorld> -- -- is not associated to any world.
Root logical volume(s) :
Pointers : G4VUserRegionInformation[0], G4UserLimits[0], G4FastSimulationManager[0], G4UserSteppingAction[0]
Materials :

PRODUCTION CUTS : GAMMA 1 NM E- 1 NM E+ 1 NM PROTON 1 MM

========== TABLE OF REGISTERED COUPLES ==========

INDEX : 0 USED IN THE GEOMETRY : YES RECALCULATION NEEDED : NO
MATERIAL : G4_WATER
RANGE CUTS : GAMMA 1 NM E- 1 NM E+ 1 NM PROTON 1 MM
ENERGY THRESHOLDS : GAMMA 0.1 EV E- 0.1 EV E+ 0.1 EV PROTON 100 KEV
REGION(S) WHICH USE THIS COUPLE :
DEFAULTREGIONFORTHEWORLD

==========

==========